ditors' Suggestion

First-Principles Nanocapacitor Simulations of the Optical Dielectric Constant in Water Ice

Anthony Mannino,[1,2] Graciele M. Arvelos,[3] Kedarsh Kaushik,[1,2] Emilio Artacho,[4,5,6] Pablo Ordejon,[7] Alexandre R. Rocha,[3] Luana S. Pedroza,[8,*] and Marivi Fernández-Serra[1,2,†]

[1]*Physics and Astronomy Department, Stony Brook University, Stony Brook, New York 11794-3800, USA*
[2]*Institute for Advanced Computational Science, Stony Brook, New York 11794-3800, USA*
[3]*Instituto de Física Teórica, Universidade Estadual Paulista UNESP), São Paulo, SP 01140-070, Brazil*
[4]*CIC Nanogune BRTA and DIPC, Tolosa Hiribidea 76, 20018 San Sebastian, Spain*
[5]*Ikerbasque, Basque Foundation for Science, 48011 Bilbao, Spain*
[6]*Theory of Condensed Matter, Cavendish Laboratory, University of Cambridge, J.J. Thomson Avenue, Cambridge CB3 0HE, United Kingdom*
[7]*Catalan Institute of Nanoscience and Nanotechnology ICN2 CSIC and BIST), Campus UAB, Bellaterra, E-08193, Barcelona, Spain*
[8]*Instituto de Física, Universidade de São Paulo, São Paulo, SP 05508-090, Brazil*

(Received 30 June 2025; accepted 2 December 2025; published 16 January 2026)

We introduce a combined density functional theory and nonequilibrium Green s function framework to compute the capacitance of nanocapacitors and directly extract the dielectric response of a subnanometer dielectric under bias. We identify that at the nanoscale conventional capacitance evaluations based on stored charge per unit voltage suffer from an ill-posed partitioning of electrode and dielectric charge. This partitioning directly impacts the geometric definition of capacitance through the capacitor width, which in turn makes the evaluation of dielectric response uncertain. This ambiguous separation further induces spurious interfacial polarizability when analyzed via maximally localized Wannier functions. Focusing on crystalline ice, we develop a robust charge-separation protocol that yields unique capacitance-derived polarizability and dielectric constants, unequivocally demonstrating that confinement alters neither ice s intrinsic electronic response nor its insensitivity to proton order. Our results lay the groundwork for rigorous interpretation of capacitor measurements in low-dimensional dielectric materials.

DOI: 10.1103/8sjg-ybfw

The dielectric response of nanoconfined water has been the subject of a large number of recent studies [1 9]. These works were mainly motivated by experimental results measuring the out-of-plane dielectric constant of water between graphene and boron nitride (BN) capacitor plates [10]. This Letter concluded that the dielectric constant of water thin films decreases with thickness from its bulk value of = 80 to a strikingly small = 2.1 for films less than 15 Å in width. Subsequent computational works have tried to understand why the polarization response of water to an external electric field in the nanoconfinement or subnanoconfinement range is so small. All of these studies relied on the determination of the dielectric constant through changes in the polarization of the thin film under an applied external field [5,11] or simulations under a constant electric displacement [2,8]. Different explanations have been proposed, ranging from the structural properties of the confined films [2] to the cancellation of anisotropic long-range dipole correlations near the confined film surfaces [12]. Very recently, however, Zubeltzu *et al.* [11] highlighted that all of these works rely on making predictions that depend on ill-defined properties when taken to the subnanoscale. At the macroscopic level, determining the dielectric constant of the material filling a capacitor is straightforward: one measures the stored charge Q on two capacitor plates of area A separated by a well-defined width w_0 when an external bias V is applied and uses

$$= \frac{C}{C_0} = \frac{Q/V}{{}_0 A/w_0} \tag{1}$$

Here, C and C_0 are the capacitances of the full and empty capacitor, ${}_0$ is the permittivity of free space, w_0 is the plate separation, and Q lives entirely on the metallic surfaces. However, when we shrink the device to the nanometer or subnanometer scale, w_0 and Q, the two key ingredients of that simple macroscopic picture, become ill defined. Here, different definitions of w_0 can vary by several angstrom leading to a 20 (or larger for a subnanometer capacitor) uncertainty in $C_0 = {}_0 A/w_0$ even before any dielectric is added [see Supplemental Material (SM) [13]]. In addition,

*Contact author: luana@if.usp.br
†Contact author: marivi.fernandez-serra@stonybrook.edu

the metal electron density spills out into the first molecular layers of the dielectric, and the polarization charge of the dielectric overlaps spatially with the metal s induced charge. Any attempt to split the total electron-density change into electrode charge and dielectric charge becomes ambiguous. Because of these two intertwined ambiguities—effective separation and charge partition—applying Eq. (1) to sub-nanometer capacitors can produce spurious results.

In this context, Zubeltzu *et al.* [11] following what was done for 2D materials [17] proposed that the true measure of dielectric response for a nanometer-thick film is the two-dimensional polarizability,

$$\alpha = \frac{^{2D}}{D}, \tag{2}$$

where ^{2D} is the dipole moment per unit area and D is the applied displacement field. One can relate α to an intrinsic of the film via

$$= \left(1 \quad \frac{\alpha}{w_f}\right)^{1}, \tag{3}$$

but here w_f—the true thickness of the dielectric film—must itself be consistently defined at the atomic scale.

All of the above motivates a fully first-principles approach in which (i) the metal electrodes electronic degrees of freedom are treated explicitly, (ii) the metal slabs can sustain different chemical potentials under bias, and (iii) no *a priori* film thickness or charge partition is assumed. While a subset of these components has been incorporated in some simulation frameworks [18 20], only recently it was shown that such computational construction can be realized with a combination of nonequilibrium Green s functions (NEGFs) to describe the open system and density functional theory to characterize the Hamiltonian of the device [21 24]. In this Letter, we show that using this methodology it is possible to accurately obtain the electronic response of a nanoconfined dielectric to an applied external bias, hence directly reproducing experimental measurements. This framework allows us to compute, under two different applied biases, V, the spatially resolved electron-density change $\rho(\mathbf{r})$ throughout both electrodes and dielectric. From $\rho(\mathbf{r})$ one can identify the exact centroids of induced charge on each electrode—thus unambiguously defining the plate separation, and isolate the polarization charge inside the dielectric by comparing with a stand-alone slab reference. In doing so, we remove any ambiguity in applying Eq. (1) or (3) at the ∼Å scale. While the methodology is general and can be applied to any type of dielectric system, we focus in this Letter on understanding the purely electronic or optical response $_{\infty}$ of hexagonal ice *Ih* and *XI* [25,26]. Note that throughout this Letter we use to refer to $_{,\infty}$. We will show that, for the electronic response, ice already reflects most of the physics that should already be present in nanoconfined water capacitors, but makes the overall analysis more simple.

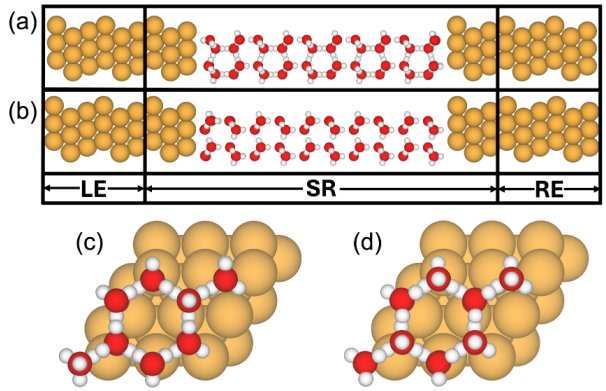

FIG. 1. Illustrations of the (a),(c) ice *Ih*-Au[111] capacitor and (b),(d) ice *XI*-Au[111] capacitor. (a),(b) Side views and (c),(d) top views. The left and right electrodes (LE and RE, respectively) and the scattering region (SR) are shown.

The simulated plate capacitors consisted of two semi-infinite Au slabs grown along the [111] direction acting as electrodes, and an ice slab [26,27] in between, with its c axis perpendicular to the Au electrode surfaces, as illustrated in Fig. 1. As described in [21,22], the system is split into three regions [28], namely, two semi-infinite electrodes, capable of sustaining a different chemical potential if a bias is applied, and a scattering region (SR), which consists of the ice slab and three layers of Au on either side. We consider two different proton order configurations for the ice slab. (i) A proton ordered structure with four molecules per unit cell with a net dipole moment along the c axis, that we coin ice *XI* as in [27]. The ice *XI* slab consists of $2 \times 2 \times 5$ repetitions of this unit. (ii) A zero-dipole moment structure, twice the size of the ice *XI* unit cell along the two in-plane directions, with also 5 unit repetitions along the c direction. We refer to this structure as the ice *Ih* slab, since it mimics the net zero dipole of proton disordered systems. Both structures are illustrated in Fig. 1. These ice slabs can be described as a stack of ten identical ice bilayers. All calculations were done using the SIESTA [29,30] code which incorporates the TRANSIESTA [24] method for NEGF calculations. We evaluate how the presented results depend on structural relaxations with and without bias in SM [13]. Additional computational details are also provided in SM [13].

For an empty Au-plate capacitor, we compute capacitance by applying a small bias difference V and integrating the induced charge in each electrode:

$$Q_0 = \int_{z_{\mathrm{in}}}^{z_{\mathrm{out}}} \rho_{V}(z)dz, \qquad C_0 = \frac{Q_0}{V} \tag{4}$$

Here the integration limits z_{in}, z_{out} are chosen where $\rho_{V}(z)$ vanishes in the bulk electrode (z_{in}) and inside

the gap region (z_{out}). The corresponding plate separation w_0 is taken as the distance between the two centroids of $\rho_V(z)$. When ice fills the gap, the total induced charge includes both electrode-surface charge and polarization charge in the ice. To isolate the electrode contribution, we first determine the uniform displacement field change D using a half-full capacitor by fitting the slope of the Hartree potential in the vacuum region, see SM [13]. We then apply that same D to an isolated ice slab to compute its polarization charge $\rho_D^{\text{slab}}(z)$. Subtracting $\rho_D^{\text{slab}}(z)$ from the half-full capacitor $\rho_V(z)$ leaves only the electrode-induced charge. This procedure assumes linearity under bias, which is demonstrated in SM [13]. It is important to note that when doing this, we assume that the polarization charge is unchanged by the presence of the metal, which is true for our ice systems, as we will show. Integrating this difference yields the true electrode charge difference Q. Comparing the induced charge Q of the full capacitor with that of the empty capacitor Q_0 fixes $^{\text{eff}}$, the effective dielectric response of the Au ice Au stack via

$$^{\text{eff}} = \frac{Cw}{C_0 w_0} = \frac{Qw}{Q_0 w_0}, \tag{5}$$

where w is defined from the charge-centroid separation of the electrode-induced charges. As we will show later, w_0 and w do not necessarily need to be the same and in general they are not, even if the interplate distance is kept constant.

To isolate the ice slab s intrinsic 2D polarizability, we use the relation [11]

$$\alpha = (w \quad w_0) + {}_0A(C_0{}^1 \quad C^{-1}) \tag{6}$$

α has units of length, and it is an extensive quantity, i.e., depends on the thickness of the measured material.

With the equations above we can compute α and $^{\text{eff}}$ using capacitance calculations from our biased Au electrode-ice devices. As our dielectric film is crystalline, it is also possible to exactly compute its intrinsic dielectric response using Eq. (3), because here $w_f = c$, the lattice parameter of the system along the normal direction.

We can also compute a spatially resolved (z) directly from the electron density using the polarization analog to Gauss s law.

$$\cdot \quad = \quad \rho(\mathbf{r}), \tag{7}$$

where is the 3D polarization vector. Given the symmetry of the parallel capacitor geometry, we can simplify this to the following form:

$$P(z) = \frac{1}{A} \int_{z_0}^{z} \bar{\rho}(z')dz', \tag{8}$$

which can then be used to calculate the out-of-plane dielectric constant as

$$(z) = \left(1 \quad \frac{P(z)}{D}\right)^{1} \tag{9}$$

The constant z_0 is determined such that diverges in the electrode. $\bar{\rho}$ is the running average of the electronic density over c. This continuous (z) mixes the dielectric constants from the metal and the ice at the interface when using $\rho_V(z)$. Using the charge partition scheme previously presented it is possible to separate it into electrode and dielectric components.

We can alternatively calculate the local dipole moments of individual molecules using Wannier functions [31], which in principle allow us to decouple the dielectric and metal electronic degrees of freedom. Then one can use the Wannier charge centers (WCCs) to compute $_{2D}$ for each bilayer (BL), and this can be used to compute α as

$$\alpha^{\text{BL}} = \frac{^{\text{BL}}_{2D}}{D} \tag{10}$$

These can then be used to compute a layer-resolved using Eq. (3).

The computed values of the optical dielectric constant for the half-full ice *Ih*-Au capacitor using the electronic density and WCCs methods are shown in Fig. 2. We also

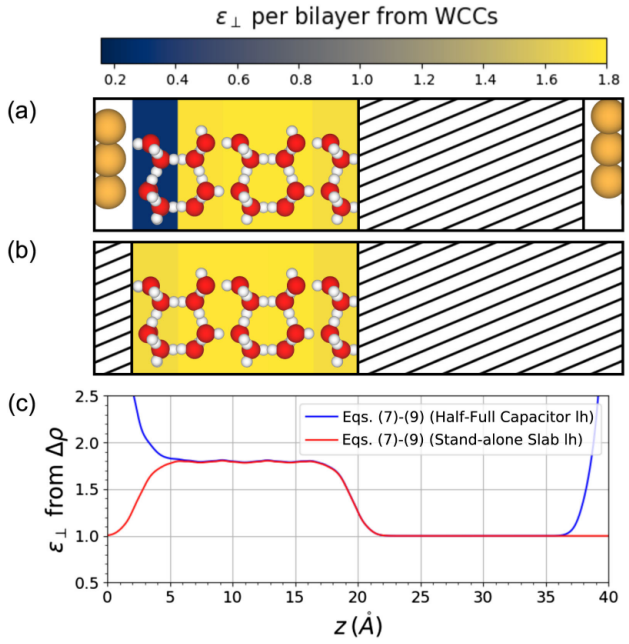

FIG. 2. Optical dielectric constant in (a) half-full capacitor and (b) stand-alone slab geometries calculated using two methods. (a),(b) The Wannier charge center (WCC) method described by Eqs. (3) and (10). (c) The electron-density method described by Eqs. (7) (9). Surface Au electrode planes are at $z = 0$ and $z = 40$ Å. In both cases finite differences are computed with $V = 1V$.

computed the optical dielectric constant using WCCs for an identical ice *Ih* slab placed in vacuum under an applied displacement field identical to that of the capacitor simulation. Results for this ice-only slab calculation are also presented in Fig. 2. In the bulk ice region, all of these methods predict ≈ 1.8, closely matching the known optical dielectric constant of ice and water [32,33]. This is expected, given that the electronic molecular polarizabilities of ice and water are almost identical [34]. This is also the reason why the computed optical dielectric constant is independent of the structural relaxation of the system under bias, as shown in SM [13].

The WCC results for the half-full capacitor shown in Fig. 2 are surprising near the metal-ice interface. They suggest that < 1 ($\alpha < 0$) near the interface, indicating an antiscreening response. This is at odds with the results for the ice slab, which only see a slight decrease in the optical dielectric constant at the interfaces. This discrepancy quickly dissipates away from the interface, with results being insensitive to the method by the third bilayer from the metal interface. According to these results, ice has a nonhomogeneous layer-by-layer polarizability when in contact with a metal. If this was the case, subtracting $\rho(z)$ for the stand-alone ice slab from $\rho(z)$ for the half-full capacitor would result in large density oscillations near the metal water interface. This is because the amplitude of the density oscillations corresponds to the difference in the dielectric response. Note that the stand-alone ice slab, which is polarized with the same displacement field as the ice slab within the capacitor, results in a uniform layer-by layer polarization. Results for this subtraction are plotted in Fig. 3. The remaining charge density difference, while not exempt of small perturbations, closely resembles the characteristics of $\rho(z)$ for the empty capacitor, which is also plotted in the Fig. 3. If the optical dielectric response near the metallic interface were much different from that of the slab, as suggested by the WCC results, we would expect to see large oscillations in the dielectric region. However, in this case the oscillations are virtually nonexistent, showing that the dielectric response of the ice within the capacitor is virtually the same as the stand-alone ice slab. This confirms our initial assumption that the polarization charge is not affected by the presence of the metal. The most noticeable change is that the electrode charge in contact with ice seems to penetrate deeper into the dielectric region than in the empty capacitor. These two charge densities can be used to compute w $w_0 =$ 0.48 Å, which is shown in Fig. 3. As mentioned earlier, atomic relaxations do not modify the value of the optical dielectric constant of ice. However, they increase the electronic charge overlap at the ice-Au interface, worsening the error in the surface layer polarizabilities computed using the WCCs. A detailed analysis of this is presented in SM [13].

Additional care needs to be taken when computing in the ice *XI* slab. This is because this system is metallic at the

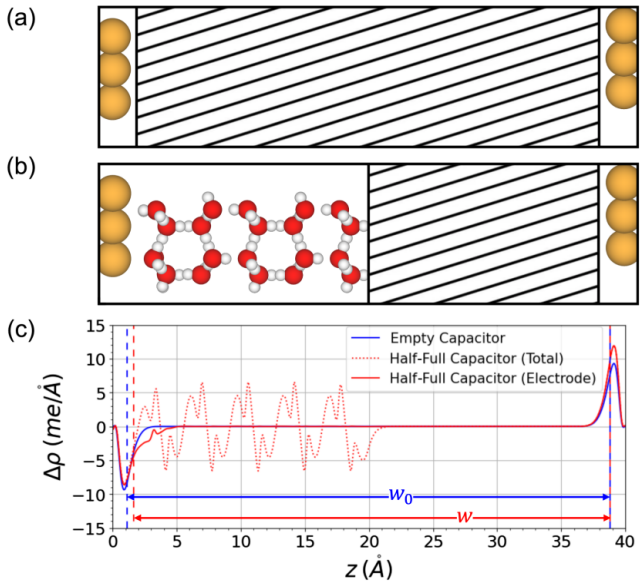

FIG. 3. Illustrations of (a) the empty capacitor and (b) the half-full capacitor geometries. (c) Electrode charge density difference for the empty capacitor (solid blue line) and the half-full capacitor (solid red line) geometries. The total charge density difference for the half-full capacitor geometry is also shown (dotted red line). Surface Au electrode planes are at $z = 0$ and $z = 40$ Å. The vertical dashed lines give the boundaries of the dielectric region, and the capacitor widths, w and w_0, for each system are labeled.

sizes we consider in this Letter (5 and 10 bilayers). This stems from inadequate screening of the ferroelectric at the ice/vacuum interface, which causes an electronic reconstruction known as the "polar catastrophe" [35]. Nonetheless, we can still compute D for the full capacitors (see SM [13]). Results are shown in Fig. 4. We find that within the bulk region is virtually the same for the two different proton ordered ices (≈ 1.8). We also see a similar suppression of the dielectric constant calculated using WCCs near the interfaces, although there seems to be a dependence on the water molecule orientation relative to the metal surface. A more detailed analysis of the errors in the WCCs and their dependence on the molecular orientation relative to the metal surface can be found in SM [13]. We find that w $w_0 =$ 0.91 Å for the full ice *Ih* capacitor. Using Eq. (6), we can compute the 2D polarizability with and without this width correction. We can then compute the effective dielectric constant and the optical dielectric constant of ice using Eq. (3). These results are shown in Table I along with similar calculations for the stand-alone ice slab. The slab results are in noticeably better agreement with the $w \neq w_0$ result, demonstrating the importance of calculating a physically meaningful width. Indeed, here the error due to using the incorrect width is only 5 for a 10 bilayer slab of net width ~36 Å. However for a slab of net width ~1 nm the error would increase to 20 .

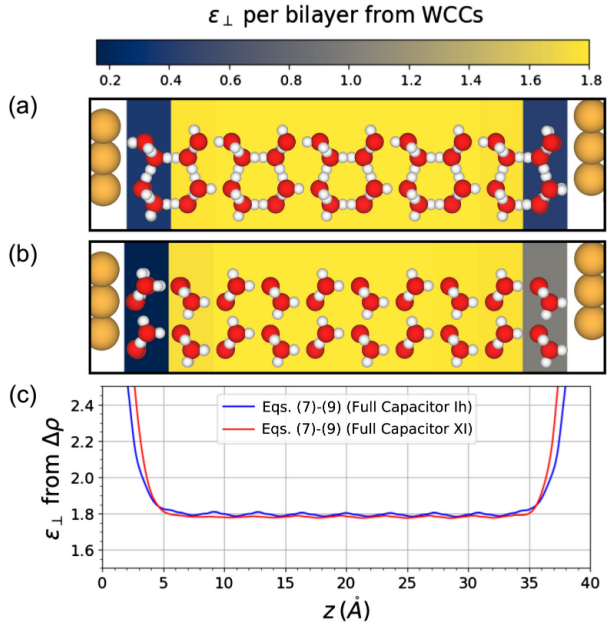

FIG. 4. Optical dielectric constant in full (a) ice *Ih* and (b) ice *XI* capacitor geometries calculated using two methods. (a), (b) The WCC method described by Eqs. (3) and (10). (c) The electron density method described by Eqs. (7) (9). Surface Au electrode planes are at $z = 0$ and $z = 40$ Å. In both cases finite differences are computed with $V = 1V$.

Our results show that nanoconfinement has a negligible effect on of ice, regardless of proton order. This is true for both a stand-alone ice slab and an ice capacitor with Au electrodes. Therefore, neither the nature of the electrodes nor confinement affect the measured *electronic* dielectric response. According to Fumagalli *et al.* [10], this behavior is expected and underlines the anomalously low value of = 2.1 measured for the electrically dead layer of a water dielectric thin film near the capacitor interface. However, recent studies [11,19] have suggested that there is a noticeably different behavior at this interface, whether it be a smaller [11] or larger [19] electronic response. Zubeltzu *et al.* [11] predict = 1.24 for a stand-alone subnanometer thin film of water. This result leads us to conclude that the reduction of the total dielectric constant seen in the work of Fumagalli *et al.* [10] can be mostly explained by the reduction in the electronic response. Zhu *et al.* [19] use similar methods to the ones we use in this Letter, but come to a different conclusion. They assume that the electrode s charge spilling is unchanged by the presence of a dielectric, i.e., $w = w_0$, and instead attribute the moderate rise (< 25) in the optical dielectric constant near the metal/water interface, calculated using the electron density, to the interfacial water molecules. This assignment uses the WCCs of the interfacial water molecules, which are found to be more diffuse and polarizable than their counterparts in the bulk region. Conversely, here we have found that the WCCs are unreliable near the interface if computed from a calculation where the electrode is not decoupled. This effect is exacerbated by the change in the capacitor geometry ($w \neq w_0$) when a dielectric is inserted.

TABLE I. Calculations of the 2D polarizability (α), effective optical dielectric constant ($^{\text{eff}}$), and intrinsic optical dielectric constant of ice *Ih* ( ) for the full ice capacitor with $w = w_0$ and $w \neq w_0$, and the stand-alone ice slab.

	α (A)	$^{\text{eff}}$ [Eq. (5)]	[Eq. (3)]
Au-Ice ($w = w_0$)	16.8 [Eq. (6)]	1.80	1.87
Au-Ice ($w \neq w_0$)	15.9 [Eq. (6)]	1.76	1.78
Ice slab	15.7 [Eq. (10)]	···	1.77
Experiment [32]	···	···	1.7 1.8

Those last two points are important to emphasize. First, we find that the WCCs are not able to adequately partition the charge between the electrode and the dielectric, leading to specious results near the interface. This is not surprising in situations like this where a very small amount of charge transfer [21,22] between the ice film and the metal takes place. This adds an extra level of care that needs to be taken in these interfacial calculations because not only is the width ill defined, but the 2D polarizability can also be ill defined if it relies on the computation of Wannier charge centers. Our results show that this effect extends up to the third bilayer from the interface (∼10 Å), which is larger than the dead layer thickness of 7.5 Å reported experimentally [10]. Second, we find that the electrode charge spills out further in the presence of a dielectric (i.e., $w < w_0$). This has significant implications on Eq. (6), which was originally derived as a way to calculate the 2D polarizability using only experimentally measurable quantities such as the capacitance [11]. The difference w w_0 was intended to be the change in the distance between the atomic planes of the electrodes. However, in our case this distance is fixed, yet we still see $w \neq w_0$. This means that Eq. (6) depends on an ill-defined width, and is no longer easy to measure experimentally.

This Letter offers a transferable strategy for interpreting experimental capacitance data in low-dimensional dielectrics, where the standard macroscopic relation [Eq. (1)] becomes only an approximate description. In this regime, we show that differential-capacitance analyses must explicitly include electrode-induced charge smoothing via Eq. (5). Beyond ice, this methodology can be directly applied to other 2D or nanoconfined materials—organic, hybrid, or oxide dielectrics—providing a rigorous route to their high-frequency dielectric characterization under realistic bias. Future extensions to include ionic contributions will further bridge toward understanding the full dielectric response in nanoscale capacitors.

Acknowledgments M. F.-S. and A. M. were funded by the National Science Foundation Award No. DMR-2427902.

A. M. thanks the Institute for Advanced Computational Science (IACS) at Stony Brook University (SBU) for support through a graduate fellowship. The authors would like to thank Stony Brook Research Computing and Cyberinfrastructure and IACS at SBU for access to the high-performance SeaWulf computing system, funded by the National Science Foundation (Awards No. 1531492 and No. 2215987) and matching funds from the Empire State Development s Division of Science, Technology and Innovation (NYSTAR) program (Contract No. C210148). L. S. P., G. M. A., and A. R. R. would like to acknowledge financial support from Fundação de Amparo à Pesquisa do Estado de São Paulo (FAPESP Grants No. 2017/10292-0, No. 2020/16593-4, and No. 2023/09820-2), Conselho Nacional de Pesquisa (CNPq), and CAPES. Some Calculations were carried out at CENAPAD-SP and at the Santos Dumont High performance facilities of Laboratorio Nacional de Computação Científica (LNCC), Brazil. E. A. was supported by the European Commission Horizon MSCA-SE Project MAMBA (Grant No. 101131245), the Spanish MCIN/AEI/10.13039/501100011033 (Grant No. PID2022-139776NB-C65), a María de Maeztu award to Nanogune (Grant No. CEX2020-001038-M), the United Kingdom s EPSRC (Grant No. EP/V062654/1), and the Basque Ikur HPC program, through a 2023 Cotutelage grant. P. O. was supported by the Spanish MCIN/AEI/10.13039/501100011033 (Grants No. PID2022-139776NB-C62 and No. PCI2022-134972-2) and by a Severo Ochoa award to ICN2 (Grant No. CEX2021-001214-S) and the EU-H2020 MaX "Materials Design at the Exascale" CoE (Grant No. 101093374).

Data availability The data that support the findings of this article are openly available [36].

[1] G. Monet, F. Bresme, A. Kornyshev, and H. Berthoumieux, Phys. Rev. Lett. **126**, 216001 (2021).
[2] T. Dufils, C. Schran, J. Chen, A. K. Geim, L. Fumagalli, and A. Michaelides, Chem. Sci. **15**, 516 (2024).
[3] F. Deißenbeck and S. Wippermann, J. Chem. Theory Comput. **19**, 1035 (2023).
[4] C. Zhang, F. Gygi, and G. Galli, J. Phys. Chem. Lett. **4**, 2477 (2013).
[5] J. Zubeltzu, F. Corsetti, M. V. Fernández-Serra, and E. Artacho, Phys. Rev. E **93**, 062137 (2016).
[6] S. De Luca, S. K. Kannam, B. Todd, F. Frascoli, J. S. Hansen, and P. J. Daivis, Langmuir **32**, 4765 (2016).
[7] A. Schlaich, E. W. Knapp, and R. R. Netz, Phys. Rev. Lett. **117**, 048001 (2016).
[8] C. Zhang, J. Chem. Phys. **148**, 156101 (2018).
[9] M. H. Motevaselian and N. R. Aluru, ACS Nano **14**, 12761 (2020).
[10] L. Fumagalli, A. Esfandiar, R. Fabregas, S. Hu, P. Ares, A. Janardanan, Q. Yang, B. Radha, T. Taniguchi, K. Watanabe *et al.*, Science **360**, 1339 (2018).
[11] J. Zubeltzu, F. Bresme, M. Dawber, M. Fernandez-Serra, and E. Artacho, Phys. Rev. Res. **7**, 043101 (2025).
[12] J.-F. Olivieri, J. T. Hynes, and D. Laage, J. Phys. Chem. Lett. **12**, 4319 (2021).
[13] See Supplemental Material at http://link.aps.org/supplemental/10.1103/8sjg-ybfw for additional information about methods and results, which includes Refs. [14 16].
[14] V. Buch, P. Sandler, and J. Sadlej, J. Phys. Chem. B **102**, 8641 (1998).
[15] E. R. Jette and F. Foote, J. Chem. Phys. **3**, 605 (1935).
[16] J. P. Perdew, K. Burke, and M. Ernzerhof, Phys. Rev. Lett. **77**, 3865 (1996).
[17] T. Tian, D. Scullion, D. Hughes, L. H. Li, C.-J. Shih, J. Coleman, M. Chhowalla, and E. J. Santos, Nano Lett. **20**, 841 (2020).
[18] Z. Ye, A. Prominski, B. Tian, and G. Galli, Proc. Natl. Acad. Sci. U.S.A. **118**, e2114929118 (2021).
[19] J.-X. Zhu, J. Cheng, and K. Doblhoff-Dier, J. Chem. Phys. **162**, 024702 (2025).
[20] L. Li, T. Eggert, K. Reuter, and N. G. Hörmann, J. Am. Chem. Soc. **147**, 22778 (2025).
[21] L. S. Pedroza, P. Brandimarte, A. R. Rocha, and M.-V. Fernández-Serra, Chem. Sci. **9**, 62 (2018).
[22] G. M. Arvelos, M. Fernández-Serra, A. R. Rocha, and L. S. Pedroza, J. Chem. Phys. **162**, 094707 (2025).
[23] A. R. Rocha, V. M. García-Suárez, S. Bailey, C. Lambert, J. Ferrer, and S. Sanvito, Phys. Rev. B **73**, 085414 (2006).
[24] M. Brandbyge, J.-L. Mozos, P. Ordejón, J. Taylor, and K. Stokbro, Phys. Rev. B **65**, 165401 (2002).
[25] T. Bartels-Rausch, V. Bergeron, J. H. E. Cartwright, R. Escribano, J. L. Finney, H. Grothe, P. J. Gutiérrez, J. Haapala, W. F. Kuhs, J. B. C. Pettersson, S. D. Price, C. I. Sainz-Díaz, D. J. Stokes, G. Strazzulla, E. S. Thomson, H. Trinks, and N. Uras-Aytemiz, Rev. Mod. Phys. **84**, 885 (2012).
[26] B. Pamuk, P. B. Allen, and M.-V. Fernández-Serra, Phys. Rev. B **92**, 134105 (2015).
[27] B. Pamuk, J. M. Soler, R. Ramírez, C. P. Herrero, P. W. Stephens, P. B. Allen, and M.-V. Fernández-Serra, Phys. Rev. Lett. **108**, 193003 (2012).
[28] C. Caroli, R. Combescot, P. Nozieres, and D. Saint-James, J. Phys. C **4**, 916 (1971).
[29] J. M. Soler, E. Artacho, J. D. Gale, A. García, J. Junquera, P. Ordejón, and D. Sánchez-Portal, J. Phys. Condens. Matter **14**, 2745 (2002).
[30] A. García *et al.*, J. Chem. Phys. **152**, 204108 (2020).
[31] A. A. Mostofi, J. R. Yates, G. Pizzi, Y.-S. Lee, I. Souza, D. Vanderbilt, and N. Marzari, Comput. Phys. Commun. **185**, 2309 (2014).
[32] V. F. Petrenko and R. W. Whitworth, *Physics of Ice* (Oxford University Press, Oxford, 1999), https://global.oup.com/academic/product/physics-of-ice-9780198518952?cc=us=en&.
[33] N. E. Hill, Trans. Faraday Soc. **59**, 344 (1963).
[34] X. Ge and D. Lu, Phys. Rev. B **96**, 075114 (2017).
[35] N. Nakagawa, H. Y. Hwang, and D. A. Muller, Nat. Mater. **5**, 204 (2006).
[36] A. Mannino, Ice_nanocapacitor_paper, 2025, https://github.com/amann8999/Ice_Nanocapacitor_Paper.